Multi-Terminal HVDC Networks - What is the Preferred Topology?

Digital Object Identifier: 10.1109/TPWRD.2013.2277552

Multi-Terminal HVDC Networks - What is the Preferred Topology?

Matthias K. Bucher, *Student Member, IEEE,* Roger Wiget, *Student Member, IEEE,*
Göran Andersson, *Fellow, IEEE,* and Christian M. Franck, *Senior Member, IEEE*

***Abstract*—This paper investigates the influence of the DC network topology with respect to two important aspects: the steady-state losses and the transient fault currents. For this, the optimal power flow in a combined AC-DC Multi-Terminal HVDC cable system based on Voltage Source Converters and the development of prospective fault currents during a pole-to-ground fault is simulated. The results prove that an evaluation of grid topologies must include both of the aforementioned aspects and that no network topology can optimize both at the same time.**

***Index Terms*—HVDC transmission, Power system planning, Power system faults, Power system simulation, PSCAD.**

I. Introduction

OFFSHORE HVDC power networks have been envisioned by academics, industry consortiums, and environmental NGOs [1]–[5] as a possible solution for the integration of the increasing offshore wind power production, which has exceeded 3200 MW in Europe [6]. Up to now, the power transmission from offshore wind farms has been based on HVDC or HVAC point-to-point connections. The latter is technically not feasible for long transmission distances and, therefore, an offshore network has to be based on HVDC interconnections. The Multi-Terminal HVDC (MTDC) network is a viable option due to advances in the HVDC technology such as higher ratings of the semiconductor devices and the development of Voltage Source Converters (VSC). Increased system redundancy, higher flexibility for power trading, and reduced investment and operational costs are expected benefits of an interconnected HVDC offshore power network.

One of the main difficulties of MTDC networks is the grid protection. For the reliable breaking of DC fault currents and the selective isolation of faulted cables, DC circuit breakers (CBs) are indispensable. Conventional AC side CBs provide adequate protection for point-to-point HVDC connections, but would not be viable for HVDC grids, as they require the de-energization of the entire system [7], [8]. There exist several concepts for DC CBs [9], [10], [2], which still have to be improved in terms of on-state losses or speed before they can be of practical use.

An important power system planning tool is the optimal power flow (OPF) calculation, which has been used for decades in case of AC systems, but has not been adapted to combined AC-DC system until recently. A sequential AC-DC power flow algorithm with fixed infeeds is described in [11] and an adaptation with variable power can be found in [12].

This paper discusses the influence of the DC network topology on the steady-state system losses in the combined AC-DC network, as well as the prospective fault current development at the cable ends during a DC side pole-to-ground fault and illustrates the fault clearance support provided by an adequate DC network layout. Moreover, possible contingencies after the fault clearance are investigated.

To do so, OPF and transient simulations are performed in a North Sea MTDC cable network with 12 terminals based on the proposed North Sea Supergrid described in [13]. This DC network is coupled to three fictitious, simplified, asynchronous AC network areas in the UK, continental Europe, and Scandinavia, allowing for power trading between the AC areas. Three of the MTDC network terminals are placed offshore and connected to large wind farms, whose power infeed varies. Four different DC network layouts are considered: radial, ring shaped, lightly meshed, and densely meshed. For each topology, the steady-state losses and transient overcurrents are given for three different ground fault scenarios, as well as post-fault contingencies after fault clearance. While cable faults are less frequent than overhead line faults, but typically permanent, it is still a condition that a future DC network needs to be prepared for. The emphasis in this paper is on pole-to-ground faults, since they are significantly more frequent compared with pole-to-pole faults [14], although the latter fault would lead to more severe conditions [15].

The paper is structured as follows: Section II explains the methodology of steady-state and transient simulations, Section III describes the implemented combined AC-DC network topologies and fault scenarios, and Section IV illustrates the results of the simulations. Section V then compares and discusses the network topologies followed by the conclusions in Section VI.

II. Methodology

For each simulation, an OPF calculation is performed first, whose resulting voltages and currents are used as initial values for the subsequent transient simulations of a pole-to-ground fault. The methodology of the two simulation steps is explained in the following paragraphs.

This work was financially supported by ABB Switzerland Ltd, Alstom Grid, Siemens AG, and the Swiss Federal Office of Energy (BfE).

The authors are with the Power Systems and High Voltage Laboratories, ETH Zurich, Zurich 8092, Switzerland (e-mail: bucher, wiget, andersson, franck@eeh.ee.ethz.ch).

Manuscript received Oct 31, 2012; revised Jun 25, 2013; accepted Jul 15, 2013

A. Steady-State Simulation

The method used to calculate the states and power flows in the whole grid is described in detail in [12]. The combined AC and HVDC OPF is based on models for the AC grid, the converters, and the DC grid, which are calculated simultaneously using an overall optimization routine. No master or local control of the converter set points is required in this steady-state optimization study and converter dynamics are neglected.

The AC grid flows are calculated according to the full flow equations and summed up at each node:

$$P_{km} = U_k^2 G_{km} - U_k U_m G_{km} \cos(\theta_k - \theta_m) - U_k U_m B_{km} \sin(\theta_k - \theta_m) \quad (1)$$

$$Q_{km} = -U_k^2 (B_{km} + B_{km}^{sh}) + U_k U_m B_{km} \cos(\theta_k - \theta_m) - U_k U_m G_{km} \sin(\theta_k - \theta_m) \quad . \quad (2)$$

Fig. 1 shows the model used for the VSC converters. An AC node (AC,c) with a short AC line is added to the AC node k, where the converter is placed. This line represents the transformer located between the node and the terminal. The new grid variables U_c and θ_c can be used to determine the active and reactive power flow through the terminal.

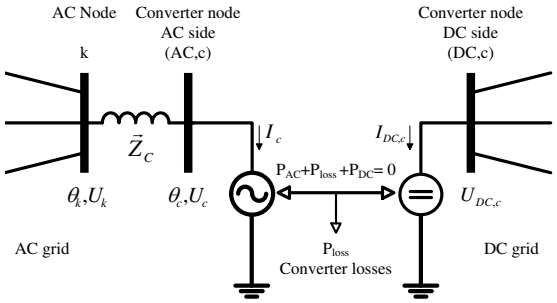

Fig. 1. VSC HVDC converter model [12]

Since the steady-state condition is investigated in these simulations, the DC grid is modeled by resistive lines only. The DC cable resistance is derived from the cable model as used in the transient simulations described in the following paragraph.

The three parts briefly described above are merged into a single, nonlinear optimization problem. To minimize the losses in the grid, the objective function is chosen in order to minimize the active power production.

The physical limits of the grid are represented by the constraints. The sum of the active and reactive power in each node has to be zero. The power on both sides of a converter and the losses in the converter itself also has to add up to zero. Inequality constraints ensure that the AC and DC voltage levels, the line loadings, and the active and reactive power production of the generators remain within fixed limits.

B. Transient Simulation

1) Solution Approach: The transients during the pole-to-ground faults in the DC network are simulated in PSCAD-EMTDC based on the Electromagnetic Transient Program (EMTP) method described in [16] and makes use of a detailed frequency dependent, distributed-parameter cable model. It allows an accurate simulation of transients in networks modeled by distributed, as well as lumped elements and permits the inclusion of the frequency dependence of the line parameters. All EMTP time domain solutions are based on the decoupling of the sending and receiving end of the transmission line given by the traveling time of the wave. Fig. 2 depicts an EMTP two-port model of the transmission line.

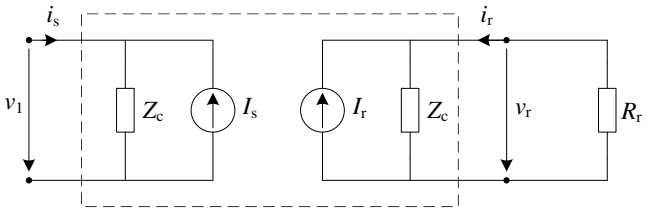

Fig. 2. EMTP transmission line model for time domain solution [17]

From Fig. 2 follow the equations for the sending end and receiving end currents using a simulation time step of Δt:

$$i_s(t) = \frac{1}{Z_c} v_1(t) - I_s(t - \Delta t) \quad (3)$$

$$i_r(t) = \frac{1}{Z_c} v_r(t) - I_r(t - \Delta t) \quad , \quad (4)$$

with the past values of the equivalent current sources

$$I_s(t - \Delta t) = \frac{1}{Z_c} v_1(t - \Delta t) - i_s(t - \Delta t) \quad (5)$$

$$I_r(t - \Delta t) = \frac{1}{Z_c} v_r(t - \Delta t) - i_r(t - \Delta t) \quad . \quad (6)$$

2) Converter and Cable Model: Identical converter and cable models as described in [18] are used for the transient simulations. The converters are modeled as a $\pm 320\,\mathrm{kV}$ bipolar two-level, half-bridge VSC topology with concentrated midpoint-grounded DC filter capacitors as depicted in Fig. 3. Each point of common coupling (PCC) of converter terminals and AC network is modeled by a separate equivalent short-circuit impedance (consisting of R_{AC} and L_{AC}) and a voltage source V_{AC}. No fault current flows through AC lines parallel to DC lines are considered. The equivalent short-circuit impedance is calculated based on the short-circuit capacity of the AC network adjacent to the PCC. In addition to the converter model in [18], the pre-fault power flow conditions resulting from the steady-state simulation are established through constant voltage sources during the pre-fault setup period. After the fault has occurred and the current at the terminal exceeds $2\,\mathrm{p.u.}$, the converters are switched to uncontrolled rectifiers as it would happen in real half-bridge based systems, when the overcurrent protection blocks the IGBTs for safety purposes [19]. The DC voltage filtering need is assumed to be low and, hence, small filter capacitors of only $1\,\mu\mathrm{F}$ are required at the DC side of each converter. This mitigates the domination of the large initial discharge currents of the concentrated filter capacitors over the distributed cable capacitances [20] and allows, consequently, for a better comparison of the different DC network topologies.

The general design of the cable cross-section is derived from a real 150 kV XLPE VSC-HVDC submarine cable [21], [22]. The cross-section was scaled up to a 320 kV cable respecting the diameter of the copper conductor [23], while keeping the electric field stress (cold condition) similar.

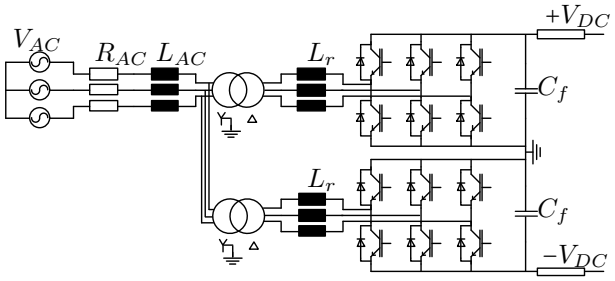

Fig. 3. Scheme of the converter model (V_{AC}: AC voltage, R_{AC}: AC resistance, L_{AC}: AC inductance, L_r: phase reactor, C_f: DC filter capacitor

III. Network Topologies and Fault Scenarios

This section describes the four proposed DC network topologies for a North Sea offshore grid and the models of the adjacent AC networks, as well as the three fault scenarios. The North Sea and its surrounding countries have been selected for this study due to the already extensive employment of offshore wind power and expansion plans in this region [6].

A. AC Network

The offshore DC grid is connected to a simplified model of an European AC grid as depicted in Fig. 4. The lines, loads, and generators are patterned on a reduced European grid map. The AC network consists of three separate, asynchronous network areas: a smaller network located in the UK, a large continental network, and a Scandinavian network, which is simplified to a single node. The grid voltage level was chosen to be 380 kV to reflect the highest level of the transmission grid, to which the DC grid will most probably be connected. Each node in the AC network represents a sub-area and has, therefore, rather high values of concentrated generation and load as listed in Table V in the Appendix. The AC line parameters are chosen from [24].

The smaller UK grid in the North West has 14 nodes and 19 lines. Its lines are between 55 km and 285 km long. The 4 generators cannot provide enough energy to supply the whole load in this scenario, hence, the 3 converter stations connected to the DC grid have to import power. Each UK node provides around 11.7 GW of short circuit power.

The larger continental AC grid comprises 23 nodes and 52 lines. On average, these lines are a little longer compared to the UK network. They have lengths between 65 km and 435 km. There is an excess in generation capacity in this area and the grid has the possibility to export power via the 5 connected converter stations into the DC grid. The continental network is stronger than the UK grid with about 43 GW of short circuit power at each node.

Node 1 has a fixed generation and represents the Scandinavian grid, which is assumed to have excess power to export.

The average distance the power has to flow from the generation to the load is rather long, therefore, the overall losses of the AC grid are high.

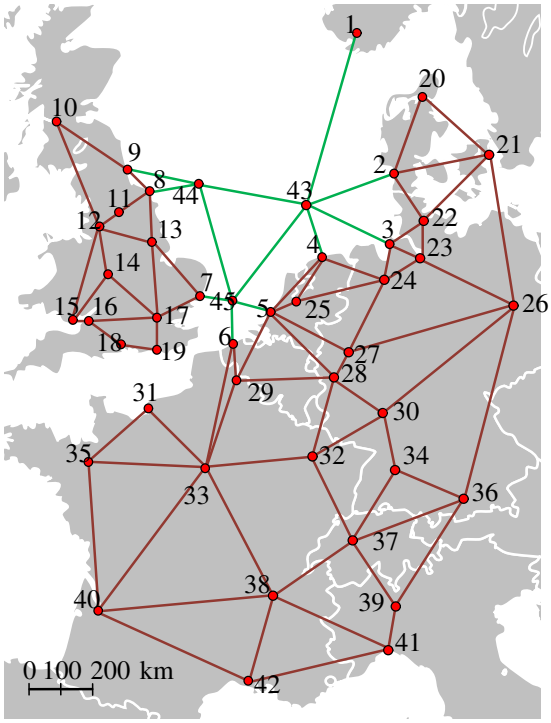

Fig. 4. AC networks (red) combined with offshore DC grid (green)

B. DC Network

Four different DC grid topologies are investigated: radial, ring, lightly meshed, and densely meshed. As illustrated in Fig. 5, all DC topologies comprise the same AC coupling points connected through 9 converter stations. Three wind parks (node numbers 43, 44, and 45) with fixed infeed are located in the DC network. The DC cable resistivity used in the OPF is $0.012304\,\Omega/\mathrm{km}$.

1) Radial Grid: Due to its simplicity and low investment cost, the radial topology will most likely be applied to a first offshore grid. It is designed like a star with the three wind parks in the center. This option (Fig. 5 A) comprises only 11 DC cables, the least number among all considered topologies, with a total length of 2270 km. In this topology, the converters are connected to only one DC cable and no DC bus bars are needed. The reliability is lower than in the other investigated topologies and it is likely to lose a complete converter station in case of a DC side fault. The radial network is assumed to be the base configuration for this paper.

2) Ring Shaped Grid: The ring topology (Fig. 5 B) connects all converter stations and wind parks in a serial circuit resulting in two DC cables per converter station. This sums up to 12 DC lines, which have a total length of 2660 km. The advantage of this topology is the simplicity for construction and operation. Obviously, the ring topology has low reliability and high losses due to the long transmission distances.

3) Lightly Meshed Grid: To slightly increase the reliability compared to the radial topology, a lightly meshed grid is investigated as well, as shown in Fig. 5 C). The additional line compared to the radial topology increases the total line length to $2590\,\mathrm{km}$. The security is only marginally increased compared with the radial network.

4) Densely Meshed Grid: The last topology is a densely meshed grid as illustrated in Fig. 5 D). Additional cables are added to the grid and the total number of cables increases to 19 with a total length of $5185\,\mathrm{km}$. The drawback of this topology is the higher cost for the long cables compared with the other topologies. The densely meshed grid increases the reliability, provides more flexibility for power exchange between the AC areas, and reduces the shortest connection distance between two points in the grid.

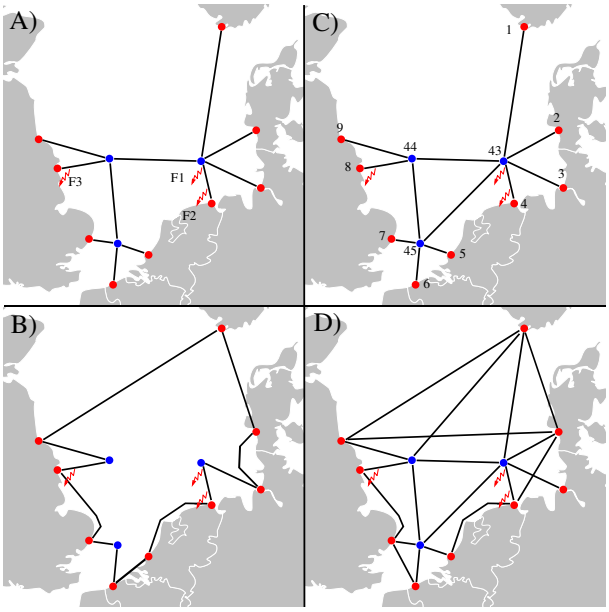

Fig. 5. DC network topologies: A) radial, B) ring, C) lightly meshed, D) densely meshed

C. Fault Scenarios

Three different ground fault locations marked by red arcs in Fig. 5 are considered: a ground fault (F1) $1\,\mathrm{km}$ away from the offshore terminal 43 on the cable connecting 43 and 4, a fault (F2) close to the strong AC coupling point 4 on the same cable, and a fault (F3) on the cable connecting nodes 44 and 8 close to a weak AC coupling point 8. Faults F2 and F3 are located $30\,\mathrm{km}$ and $50\,\mathrm{km}$ away from terminal 4 and 8, respectively. In all fault scenarios, a constant fault resistance R_f of $7\,\Omega$ is assumed, which corresponds to the ground resistance of a sparking ground connection in wet, loamy sand at the current peak of $19.35\,\mathrm{kA}$ [25]. The dependence of the fault resistance on the fault current is neglected in all the simulations. The prospective fault currents are measured at the feeder CB locations at cable $43 \rightarrow 4$ in case of F1 and F2 and at cable $44 \rightarrow 8$ during F3.

IV. Simulation Results

Pre-fault steady-state, transient, and post-fault steady-state simulations have been performed for all scenarios and topologies, whose results are presented in the following.

A. Pre-Fault OPF

For the four topologies, all generators in the UK grid are nearby or at their capacity limits. The additional load of about 22.4 % of the UK power is imported over the DC grid. Therefore, converters 7, 8 and 9 are mainly importing as shown in Fig. 6 in per unit with a base power of S_b = 1 GW. In continental Europe, converter station 2 imports power from the DC grid and all other converters export power into the DC grid. The wind park nodes have the same power infeeds for all topologies. The resulting active power losses are indicated in Table I, which reveals that the overall system losses are dominated by the converter and the AC line losses in all topologies.

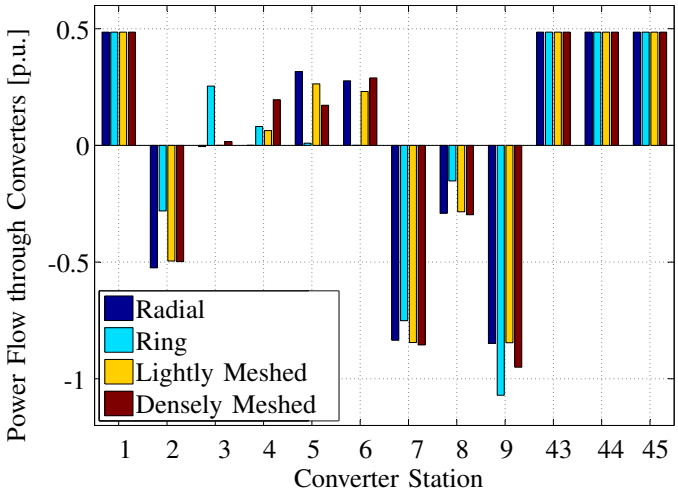

Fig. 6. Converter power flows on DC side [p.u.]

1) Radial Network: None of the DC cables reaches its capacity limit of $0.9\,\mathrm{p.u.}$, but the capacity margins of cables 9 to 44 and 7 to 45 are small. Similar to the highest line loading, the converter at node 7 has the highest loading of all terminals as given in Table II. The active power losses of the system are summarized in Table I.

2) Ring Network: The ring topology results in a completely different OPF. It is the only case, where node 1 is not at the maximum DC voltage level, but node 3 instead. On the other side of the DC grid, the lowest voltage level is at node 9, which is also the most loaded node with an import of over $1\,\mathrm{p.u.}$. The DC grid reaches its limitation as the cable from node 45 to 7 is at its capacity limit. The power flows in the other lines are far below their limits. The overall losses are the highest among all topologies: the increase in the losses is about 4 % in the DC network and about 7 % in the continental grid compared with the base case. The power flows through the converters are significantly distinct from all other topologies.

3) Lightly Meshed Network: The lightly meshed topology gives almost the same results as the radial network. This is not surprising due to the similar layout. The individual power losses and flows are almost equal to the radial network and the overall losses are reduced by only 0.26 %. A larger difference can be found in the DC line loadings, which could

be reduced by 2.88 %. There is a slight change in the infeed from converters 5 and 6.

4) Densely Meshed Network: The densely meshed topology has the lowest overall losses that are about 3.7 % lower than in the radial topology. The most significant difference is in the DC grid power losses, which are reduced by more than 50 % due to the shorter transmission distances. This results in the smallest DC voltage differences between the nodes. In this case, it is even possible to transfer more power from the wind parks through the DC grid to the UK than actually required and allows for the reduction of the loading of one of the UK's generators.

TABLE I
PRE-FAULT ACTIVE POWER LOSSES IN THE GRID [P.U.]

	DC Grid		AC Lines		Total losses	
	Converters	Lines	UK	Continental	p.u.	relative
Radial	0.1688	0.0300	0.1213	0.1223	0.4644	1.0383
Ring	0.1692	0.0312	0.1178	0.1308	0.4723	1.0561
Lightly Meshed	0.1684	0.0291	0.1213	0.1225	0.4631	1.0356
Densely Meshed	0.1716	0.0144	0.1147	0.1225	0.4472	1.0000

TABLE II
LINE LOADINGS [P.U.]

	Highest loaded DC line	Power transfer	Highest loaded AC line	Power transfer
Radial	44 to 9	0.84835	12 to 11	0.76390
Ring	45 to 7	0.89497	12 to 11	0.74683
Lightly Meshed	99 to 9	0.84568	12 to 11	0.76703
Densely Meshed	45 to 7	0.56504	12 to 11	0.71120

B. Transient Simulations

The development of the prospective fault current in the CB at cable $43 \rightarrow 4$ next to terminal 43 during fault 1 is depicted in Fig. 7 for the 4 topologies. Right after the fault occurrence at $0\,\mathrm{ms}$, a very steep peak can be observed due to the discharge of the concentrated filter capacitor of the converter at terminal 43 and the distributed cable capacitances of the neighboring feeders at the same bus. The forward and backward traveling surges result in subsequent smaller peaks. After the capacitor has been discharged, the current decreases, followed by a gradual increase due to the AC infeeds through the converters. To estimate the amplitude of the short circuit current that a CB needs to interrupt, two grey lines are plotted in Fig. 7. Full solid state or fast hybrid CBs would break the current within about $2\,\mathrm{ms}$ (indicated by the thick grey line "S"), but these CB types typically have high on-state losses. Metal contact CBs, such as active or passive resonance CBs have almost no on-state losses, but the break time is about $50 - 60\,\mathrm{ms}$ as indicated by "R" [18]. Fig. 8 illustrates the maximum fault currents at the fault location and their individual shares that flow through the DC CBs at both ends of the faulty cable. The maximum currents are indicated for each fault scenario and DC network topology, as well as for the two different DC CB technologies. The maximum fault currents correspond to the sum of the current flows at both ends of the cable. In Fig. 8, the bars corresponding to the maximum currents in the CB closest to the fault are opaque and the values of the remote CB are shown with stacked, transparent bars. The topologies are distinguished by the following bar colors: blue (radial), cyan (ring), yellow (lightly meshed), and red (densely meshed).

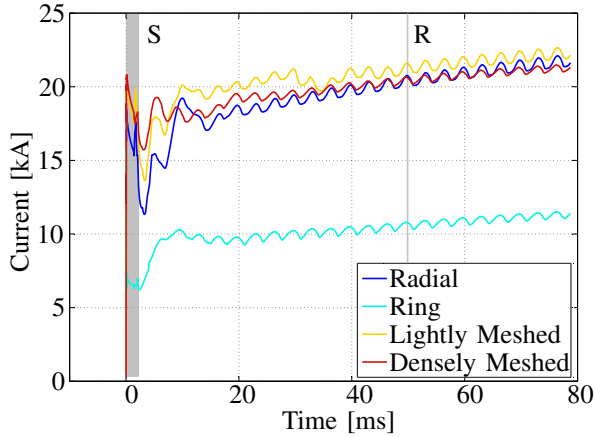

Fig. 7. CB current at terminal 43 during fault 1 - S: solid state CB, R: resonance CB

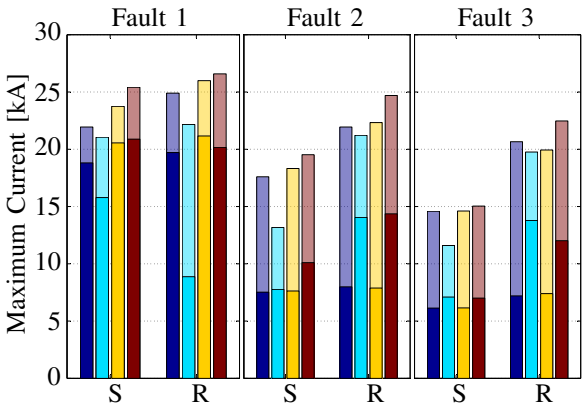

Fig. 8. Maximum fault current and individual CB currents for solid state CB (S) and resonance CB (R) - opaque bars: CB closest to fault; stacked, transparent bars: remote CB

1) Fault 1: This fault is the most severe amongst the three scenarios and results in the highest fault currents, as can be seen in Fig. 8 (left). The ring topology has the lowest fault current level and the densely meshed configuration the highest fault current contributions. The radial and lightly meshed layouts result in slightly lower fault current levels as compared to the densely meshed topology. The CB at terminal 43 (opaque bars) has to withstand almost the entire fault current given the location very close to the fault. The breaking currents at both ends of the cable are increased moderately for longer breaking times except in the ring topology, where a larger breaking time leads to a lower maximum at terminal 43.

2) Fault 2: A ground fault close to a strong AC coupling point results in lower total fault currents than in fault 1. The same tendencies as in fault scenarios 1 can be observed in Fig. 8 (center) in terms of current increase with an increase in the breaking time. The densely meshed topology yields the highest values of total fault current, whereas the ring shaped network results in the lowest contributions. In contrast to the previous fault 1, the ring network (cyan) has a relatively high

total fault current level in comparison to the other topologies. The radial (blue) and the lightly meshed (yellow) topologies lead to no increase in the maximum breaker current at terminal 4 (opaque bars) with an increase in the interruption time, whereas a considerable increase can be observed in the other two topologies. The opposite is true for the remote CB at terminal 43 (transparent bars).

3) Fault 3: The ground fault close to a weak AC coupling point (cf. Fig. 8 (right)) yields a similar result of the maximum fault currents as compared to fault 2, whereas the overall fault current levels are reduced as expected. In contrast to the previous two scenario, the lightly meshed topology (yellow) performs slightly better than the radial grid (blue). The ring shaped network (cyan) remains the topology of choice and the same fault current distribution among the CBs at both ends of the faulty cable as during fault 2 is observed.

C. Post-Fault OPF

It is assumed that the fault is cleared by opening the DC CB at both ends of the faulted cable. Since the fault is permanent, it is not possible to re-close the CBs and a re-dispatch of the power flows is required. The connected VSC converter is still in operation to provide reactive power to the AC network, even if there is no more DC line connected.

1) Fault 1 and 2: After fault 1 and 2, the cable between node 43 and 4 has been disconnected and the same post-fault OPFs are achieved for both fault scenarios. In the radial topology, as indicated in Table III, the power flows and losses remain almost the same before the fault and after fault clearance due to the negligible pre-fault power flow through converter 4 as seen in Fig. 6. The lightly meshed topology is similar to the radial layout. The small input to the DC grid at converter 4 is mainly shifted to converter 3. The overall system losses are marginally increased.

More significant changes occur in the ring topology. The highest DC voltage is shifted from node 3 to 43, since this wind park is now only connected through a single line. The infeeds at all continental terminals are increased except for node 3, where it has decreased. Node 2 has almost doubled its export to the DC grid. This leads to different infeeds into the UK grid: the power flow through converter 7 and 9 has decreased and in node 8 increased. The post-fault system losses are 2 % smaller due to the lower losses in the continental AC grid, which have declined by 5.4 % given the higher flexibility in the open ring topology. In addition, the DC lines have 7.5 % lower losses, whereas the converter losses remain equal and the losses in the UK AC grid increase slightly.

The densely meshed topology can compensate for the loss of the faulted cable without major disturbance in the system, therefore, the flows and overall losses in the grid are similar for the pre- and post-fault OPF.

2) Fault 3: After fault 3, the connection between node 44 and 8 is opened. The radial and lightly meshed topology cannot provide the required imports to the UK grid anymore due to the power limitation of the remaining DC cables. Major disturbances including load-shedding and power outages are likely. The wind park at node 44 provides the required imports in the ring topology. As after fault 1 and 2, the open ring is more flexible than the closed one and, hence, the losses are slightly smaller. The power flows in the densely meshed topology can be re-routed through many alternative lines. This results again in an almost equal flow and loss situation as before the fault.

TABLE III
CHANGES IN ACTIVE POWER LOSSES AFTER THE FAULT [%]

Fault		DC Grid		AC Lines		Total
		Converters	Lines	UK	Continental	Losses
1 and 2	Radial	-0.020	0.007	0.023	0.028	0.005
	Ring	-0.070	-7.547	1.119	-5.419	-1.879
	Lightly Meshed	0.032	-0.842	0.002	0.260	0.048
	Densely Meshed	-0.180	10.145	0.548	0.074	0.376
3	Ring	1.277	-5.971	-0.743	-4.928	-1.201
	Densely Meshed	0.562	12.680	-0.369	-0.274	0.645

V. COMPARISON AND DISCUSSION

The results achieved in this paper are summarized in Table IV. The different topologies are ranked according to their performance from the best result (1) to the worst (4). The results for steady-state and transient performance are not congruent as discussed in the following paragraphs. There is no optimal network topology, which minimizes steady-state losses and transient overcurrents at once, and each topology has its drawbacks.

TABLE IV
COMPARISON OF PERFORMANCE

	Pre-Fault OPF	F1	F2	F3	Post-Fault OPF
Radial	3	2	2	3	4
Ring	4	1	1	1	2
Lightly Meshed	2	3	3	2	4
Densely Meshed	1	4	4	4	1

A. Steady-state operation

The preferred scheme for the optimal power flow and overall losses is the densely meshed grid. After the fault, only minor changes occur in this topology. This is a clear operational advantage over all other topologies. A major drawback is the increased total cable length, which leads to much higher costs compared with other topologies. The radial and lightly meshed grid yield similar power flow results given their almost equal structure. The additional line in the lightly meshed network provides marginally better results. The comparison of pre- and post-fault results in the ring topology exhibits an interesting aspect: before the fault occurs, the ring is inflexible due to the fixed voltage distribution. It results in the highest losses amongst the considered topologies. After one line is disconnected, however, the degree of freedom is increased and a better solution can be found.

The radial topology will most likely be applied to a first offshore grid connecting large wind parks. This grid will be mainly used to transfer the offshore produced power to the onshore grids. To increase the capacity for the power exchange between the grids, particularly during no-wind conditions, and enhance the reliability and flexibility, the grid has to

be transformed in a lightly meshed network in a next step. Later on, it has to be investigated, which level of meshing is reasonable for a further increase of capacity and reliability and expands the network towards a densely meshed grid.

B. Transient overcurrents

As shown in Fig. 8, the total fault current, i.e. the total height of the bars, increases with decreasing distance to the fault and increasing short circuit capacity of the AC network at the PCC of the onshore terminals (cf. node numbers 1-9 in Fig. 4). Therefore, fault 1 has the highest values ($1\,\mathrm{km}$ between CB and fault) and fault 3 the lowest values (weak AC node and $50\,\mathrm{km}$ between CB and fault).

In all fault scenarios and topologies, a solid state CB would have to break a lower fault current than a resonance CB. The reason for that is the low initial discharge peak given the small DC filter capacitor size in this setup and the slow increase of the AC infeed currents limited by the AC impedances. As depicted in Fig. 7, the fault current still increases after $50\,\mathrm{ms}$. The steady-state fault current is reached after $200 - 300\,\mathrm{ms}$ and thus, a slower CB would have to break an even higher current than the resonance CB.

In terms of total fault current level, the ring topology performs best among all topologies considered in this paper. The reason for the good performance of the ring network is the low and evenly distributed number of feeders per busbar at the terminals. Fewer feeders at the busbars reduce the total distributed cable capacitance that may be discharged through the busbar and CB into the ground fault, as well as the lower short circuit power at the specific node given the reduced number of connections to the onshore AC nodes. Moreover, the ring reduces considerably the maximum current in the closest CB at terminal 43 during fault 1 at the cost of an increased maximum value in the remote CB at terminal 4. This is due to the equal number of feeders and similar short circuit power at the two terminals of the faulted cable.

The densely meshed topology, in contrast to the ring network, exhibits the highest fault current values due to the increased number of feeders per busbar and shorter transmission distances to the AC nodes.

The ring and densely meshed grid are unfavorable for the CBs close to fault 2 and 3 at terminals 4 and 8, respectively, whereas the radial and lightly meshed network support them, particularly in case of long breaking times. The additional connections at the network's periphery in the ring and densely meshed networks lead to a re-distribution of the fault current at both terminals of the faulted cable and yield higher breaking currents in the closest CBs on one hand and lower currents in the remote CB on the other hand.

VI. Conclusions

The paper has discussed aspects of steady-state OPF and transient simulations in a large, combined AC/DC network. The simulations have been performed for four different DC network topologies and three different ground fault locations. All scenarios have been evaluated and compared in terms of overall system losses, transient fault currents, and post-fault contingencies. It has been demonstrated that an evaluation of grid topologies has to be done taking into account all of the aforementioned aspects. On the one hand, a ring shaped topology performs best in terms of transient overcurrents due to the low and equally distributed number of feeders per busbar, but has large overall system losses in the steady-state operation given the long transmission distances and the low number of cables. After clearing the fault and disconnecting the faulted cable, contingencies are very likely. On the other hand, a densely meshed grid provides low system losses, but high transient overcurrents, because of the increased number of feeders per busbar and short transmission distances to strong AC nodes. In terms of reliability and flexibility for power exchange, it is the best choice, whereas the investment costs are highly elevated due to the large number of cables and high converter ratings. Moreover, the short circuit power at the onshore AC nodes has to be considered in order to reduce fault current levels. No DC topology can optimally satisfy all aspects at the same time and individual calculations have to be done for every network and power flow scenario. The impact of a change in the overall setup including AC networks and power flow scenarios, e.g. a DC overlay grid with several parallel AC lines, has to be investigated in future studies.

Appendix

See Table V.

References

[1] D. van Hertem and M. Ghandhari, "Multi-terminal vsc hvdc for the european supergrid: Obstacles," *Renewable and Sustainable Energy Reviews*, vol. 14, no. 9, pp. 3156–3163, 2010.

[2] D. Jovcic, D. van Hertem, K. Linden, J.-P. Taisne, and W. Grieshaber, "Feasibility of dc transmission networks," in *Proc. IEEE ISGT Europe*, Manchester, UK, Dec. 2011, pp. 1–8.

[3] Friends of the Supergrid FOSG WG2. (2012, Mar.) Roadmap to the supergrid technologies. Final Report. [Online]. Available: http://www.friendsofthesupergrid.eu

[4] OffshoreGrid. (2011, Oct.) Offshore electricity grid infrastructure in europe. Final Report. [Online]. Available: http://www.offshoregrid.eu

[5] Greenpeace and 3E. (2008, Sep.) A north sea electricity grid revolution. [Online]. Available: http://www.greenpeace.org

[6] Lindoe Offshore Renewable Center (LORC). (2011) Knowledge center. [Online]. Available: http://www.lorc.dk/knowledge

[7] L. Tang and B.-T. Ooi, "Locating and isolating dc faults in multiterminal dc systems," *IEEE Trans. Power Del.*, vol. 22, no. 3, pp. 1877–1884, 2007.

[8] W. Long, J. Reeve, J. McNichol, R. Harrison, and D. Fletcher, "Consideration for implementing multiterminal dc systems," *IEEE Trans. Power App. Syst.*, vol. PAS-104, no. 9, pp. 2521–2530, 1985.

[9] C. M. Franck, "Hvdc circuit breakers: A review identifying future research needs," *IEEE Trans. Power Del.*, vol. 26, no. 2, pp. 998–1007, 2011.

[10] J. Haefner and B. Jacobson, "Proactive hybrid hvdc breakers - a key innovation for reliable hvdc grids," in *Proc. CIGRE Symposium*, Bologna, Italy, Sep. 2011.

[11] J. Beerten, S. Cole, and R. Belmans, "A sequential ac/dc power flow algorithm for networks containing multi-terminal vsc hvdc systems," in *Proc. IEEE PES General Meeting*, Minneapolis, USA, 2010.

[12] R. Wiget and G. Andersson, "Optimal power flow for combined ac and multi-terminal hvdc grids based on vsc converters," in *Proc. IEEE Power Energy Society General Meeting (PES GM'12)*, San Diego, USA, 2012.

[13] European Wind Energy Association (EWEA). (2009, Sep.) Oceans of opportunity - ewea's 20 year offshore network development master plan. [Online]. Available: http://www.ewea.org

[14] J. Candelaria and J.-D. Park, "Vsc-hvdc system protection: A review of current methods," in *Proc. IEEE Power Systems Conference and Exposition (PSCE)*, Phoenix, USA, Mar. 2011, pp. 1–7.

TABLE V
BUS DATA [P.U.]

Bus	Active Power				Reactive Power			
		Generation				Generation		
Nr.	Load	Fix	Min	Max	Load	Fix	Min	Max
1	-	0.50	-	-	-	-	-0.01	0.40
2	0.50	-	-	-	0.03	-	-0.20	0.40
3	0.30	-	-	0.50	0.03	-	-0.20	0.40
4	0.50	-	-	1.20	0.03	-	-0.20	0.40
5	-	-	-	1.20	-	-	-0.20	0.40
6	-	-	-	1.20	-	-	-0.20	0.40
7	0.50	-	-	-	0.03	-	-0.20	0.40
8	1.00	-	-	1.50	0.03	-	-	-
9	1.00	-	-	-	0.03	-	-0.20	1.00
10	0.50	-	-	-	0.03	-	-0.20	1.00
11	1.00	-	-	-	-	-	-	-
12	0.80	-	-	3.00	0.04	-	-0.20	1.00
13	0.50	-	-	-	0.03	-	-0.20	1.00
14	0.50	-	-	-	0.03	-	-	-
15	0.50	-	-	-	0.03	-	-0.20	1.00
16	0.50	-	-	1.50	0.03	-	-	-
17	1.00	-	-	1.00	0.05	-	-0.20	1.00
18	0.50	-	-	-	0.03	-	-0.20	0.50
19	0.50	-	-	-	0.03	-	-0.20	1.00
20	0.50	-	-	-	0.03	-	-0.20	1.00
21	1.00	-	-	1.50	0.05	-	-0.20	1.00
22	-	-	-	3.00	-	-	-0.20	1.00
23	0.80	-	-	-	0.04	-	-	-
24	1.00	-	-	3.00	0.10	-	-0.20	0.50
25	1.00	-	-	-	0.05	-	-	-
26	1.00	-	-	1.50	0.05	-	-0.20	1.00
27	1.00	-	-	3.00	0.10	-	-	-
28	0.80	-	-	-	0.04	-	-0.20	1.00
29	-	-	-	3.00	-	-	-0.20	1.00
30	0.50	-	-	0.60	0.03	-	-0.20	1.00
31	-	-	-	3.00	-	-	-	-
32	-	-	-	3.00	-	-	-0.20	0.30
33	1.00	-	-	-	0.05	-	-0.20	0.30
34	0.50	-	-	0.60	0.03	-	-	-
35	0.50	-	-	0.60	0.03	-	-0.20	0.50
36	0.80	-	-	1.20	0.04	-	-0.20	0.50
37	0.50	-	-	3.00	-	-	-0.20	0.40
38	1.00	-	-	3.00	0.10	-	-	-
39	0.50	-	-	-	0.03	-	-	-
40	0.80	-	-	1.20	0.04	-	-0.20	1.00
41	0.80	-	-	1.20	0.04	-	-	-
42	0.50	-	-	-	0.03	-	-0.20	0.50
43	-	0.50	-	-	-	-	-0.20	0.20
44	-	0.50	-	-	-	-	-0.20	0.20
45	-	0.50	-	-	-	-	-0.20	0.20

[15] J. Yang, J. Fletcher, and J. O'Reilly, "Short-circuit and ground fault analysis and location in vsc-based dc network cables," *IEEE Trans. Ind. Electron.*, vol. 59, no. 10, pp. 3827–3837, 2012.

[16] H. W. Dommel, "Digital computer solution of electromagnetic transients in single-and multiphase networks," *IEEE Trans. Power App. Syst.*, vol. PAS-88, no. 4, pp. 388–399, 1969.

[17] J. A. R. Macias, A. G. Exposito, and A. B. Soler, "A comparison of techniques for state-space transient analysis of transmission lines," *IEEE Trans. Power Del.*, vol. 20, no. 2, pp. 894–903, 2005.

[18] M. K. Bucher, M. M. Walter, M. Pfeiffer, and C. M. Franck, "Options for ground fault clearance in hvdc offshore networks," in *Proc. IEEE Energy Conversion Congress and Exposition (ECCE)*, Raleigh, USA, Sep. 2012.

[19] J. Yang, J. Fletcher, and J. O'Reilly, "Multiterminal dc wind farm collection grid internal fault analysis and protection design," *IEEE Trans. Power Del.*, vol. 25, no. 4, pp. 2308–2318, 2010.

[20] M. K. Bucher and C. M. Franck, "Shares of fault current sources in multi-terminal hvdc cable networks," *IEEE Trans. Power Del.*, 2012, submitted for review.

[21] L. Ronstrom, M. Hoffstein, R. Pajo, and M. Lahtinen, "The estlink hvdc light transmission system," in *Proc. CIGRE Regional Meeting on Security and Reliability of Electric Power Systems*, Tallinn, Estonia, Jun. 2007.

[22] T. Worzyk, Ed., *Submarine Power Cables: Design, Installation, Repair, Environmental Aspects*. Springer Publishing Company, 2009.

[23] ABB High Voltage Cables. (2006, Oct.) Hvdc light cables - submarine and land power cables. [Online]. Available: http://library.abb.com

[24] P. Kundur, *Power System Stability and Control*, ser. Epri Power System Engineering Series. McGraw-Hill, 1994.

[25] J. Wang, A. C. Liew, and M. Darveniza, "Extension of dynamic model of impulse behavior of concentrated grounds at high currents," *IEEE Trans. Power Del.*, vol. 20, no. 3, pp. 2160–2165, 2005.

Matthias K. Bucher (S'12) received his BSc degree and MSc degree in electrical engineering from the ETH Zurich, Switzerland, in 2009 and 2011, respectively. He joined the High Voltage Laboratory of ETH Zurich in 2011, where he is currently working towards a PhD. His research is dedicated to transients in multi-terminal HVDC networks.

Roger Wiget (S'11) was born in Lucerne, Switzerland. He received his BSc degree in electrical engineering and MSc degree in Energy Science and Technology from the ETH Zurich, Switzerland, in 2009 and 2011. He joined the Power Systems Laboratory of ETH Zurich, Switzerland in 2011 where he is working towards a PhD. His research is dedicated to HVDC networks.

Göran Andersson (M'86, SM'91, F'97) obtained his M.S. (1975) and Ph.D. (1980) degrees from the University of Lund, Sweden. In 1980 he joined ASEA's, now ABB's, HVDC division in Ludvika, Sweden, and in 1986 he was appointed full professor in electric power systems at KTH (Royal Institute of Technology), Stockholm, Sweden. Since 2000 he is full professor in electric power systems at ETH Zurich (Swiss Federal Institute of Technology), where he also heads the powers system laboratory. His research interests include power systems dynamics and control, power markets, and future energy systems. Göran Andersson is a fellow of the Royal Swedish Academy of Sciences, and of the Royal Swedish Academy of Engineering Sciences. He is Editor-in-Chief of IET Proceedings Generation, Transmission and Distribution, and the recipient of the IEEE PES Outstanding Power Educator Award 2007 and of the George Montefiore International Award 2010.

Christian M. Franck (M'04, SM'11) received a diploma in physics from the University of Kiel, Germany in 1999 and PhD in physics from the University of Greifswald, Germany in 2003. He was with the Swiss corporate research center of ABB from 2003-2009 as a Scientist and Group Leader for gas circuit breakers and high-voltage systems. Currently, he is Assistant Professor for High Voltage Technology at the Swiss Federal Institute of Technology (ETH), Zurich, Switzerland.